Search for pressure-induced tricriticality in Cr

A. Schade,[1,*] T. Adams,[1] A. Chacón,[1] R. Georgii,[1,2] C. Pfleiderer,[1] and P. Böni[1,†]
[1]*Physik-Department, Technische Universität München, 85748 Garching, Germany*
[2]*Heinz Maier-Leibnitz Zentrum (MLZ), Technische Universität München, 85748 Garching, Germany*

(Received 21 November 2018; revised manuscript received 2 April 2019; published 22 July 2019)

We investigate the possibility of reducing the phase space of magnetic fluctuations at the weakly first-order Néel transition in Cr by neutron diffraction to test whether a second-order phase transition can be induced under the application of uniaxial pressure. Using an improved setup to reduce stress inhomogeneities we succeed in increasing significantly the pressure range until irreversible broadening due to plastic deformation occurs compared with previous studies. Despite the observed tripling of the intensity of the magnetic Bragg peak $(0, 0, 1-\delta)$ at $p_{[110]} \geqslant 450$ bar, indicating a full population of a single-$\mathbf{Q}_{\pm}$-domain state, no hints of a tricritical point are observed, i.e., the phase transition remains weakly first order. Therefore, the reduction in the phase space of the magnetic fluctuations by uniaxial pressure does not lead to the predicted second-order phase transition.

DOI: 10.1103/PhysRevB.100.035122

I. INTRODUCTION

Phase transitions are of great interest in contemporary physics because they involve remarkable changes in materials' properties. Depending on the order of the transition, the thermodynamic observables change abruptly or continuously and may involve fluctuations which act as precursors to an ordered state [1] or may even stabilize new ordered phases. A prominent example is the stabilization of the skyrmion phase in helical MnSi by entropy-driven magnetic fluctuations [2]. Of particular interest are transitions where the phase space of the fluctuations is so large that a putative second-order phase transition becomes first-order [3,4]. Indeed, it was shown recently that the phase transition from the helimagnetic to the paramagnetic phase in MnSi is a fluctuation-induced first-order transition of the Brazovskii type [5].

First-order phase transitions which involve fluctuations are not uncommon. For example, at the interface ice-water and Salol, order-disorder fluctuations have been observed by means of dynamic light scattering [6,7]. There are several other first-order phase transitions, for example, in Cr, Eu, and UO_2 to name a few, that may involve fluctuations [8]. Bak *et al.* have considered whether symmetry considerations not only are useful for the classification of second-order phase transitions but also can be used for predicting first-order phase transitions. Based on the renormalization-group equations in $4-\epsilon$ dimensions they conclude that the lack of a stable fixed point may be evidence of the occurrence of a first-order phase transition [9].

According to universality, the critical behavior of the static properties and of the fluctuations near second-order phase transitions depends only on a small number of parameters of the system such as the spatial dimensionality, the number of components of the order parameter, and the symmetry of the Hamiltonian [9]. Of particular interest are systems where the phase transitions involve an increase in the unit cell, which are described by $n \geqslant 4$ vector models. Prominent examples are Cr and MnSi. Cr involves $n = 12$ [10] or even $n = 18$ components if the longitudinal fluctuations are taken into account [11]. According to Bak and Jensen, including anisotropy, MnSi exhibits $n = 8$ components [12]. Indeed, renormalization-group theory predicts for Cr and MnSi first-order phase transitions as observed experimentally in Refs. [13] and [14], respectively. Here, due to the large n, the phase space of the critical fluctuations is so large that the system circumvents the critical point and realizes a weak first-order phase transition.

A convenient tool to influence the symmetry of a system, thereby reducing the phase space of the fluctuations, is the application of an external magnetic field. Indeed, it was shown that the application of a field of $\mu_0 H_{\mathrm{TCP}}^{\mathrm{int}} = 340$ mT in MnSi induces a tricritical point at $T_{\mathrm{TCP}} = 28.5$ K [15–18]. In Cr, the application and removal of a field of 4 T leads to neither a single-$\mathbf{Q}$ nor a cubic state [13]. One of the reasons is that the coupling of the magnetic field to the spin density wave (SDW) is very weak at the Néel transition [19]. In contrast, the dilution of Cr is a very sensitive means to change the nature of the phase transition: Doping Cr with 0.5 at% V leads already to a continuous transition [20]. It is, however, not clear how homogeneous the doping is and how it affects the electronic band structure of Cr.

In the light of the above results, breaking the cubic symmetry by the application of uniaxial pressure seems to be the most convenient route to affect the order of the Néel transition of Cr. Based on the Landau-Ginzburg-Wilson Hamiltonian proposed by Bak and Mukamel [10], Barak and Walker [11] predicted that the application of uniaxial pressure along the [110] direction in Cr leads to a reduction in the symmetry of the order parameter. Thus the available phase space for fluctuations is reduced. Therefore, the order of the Néel transition

*a.schade@tum.de
†peter.boeni@frm2.tum.de

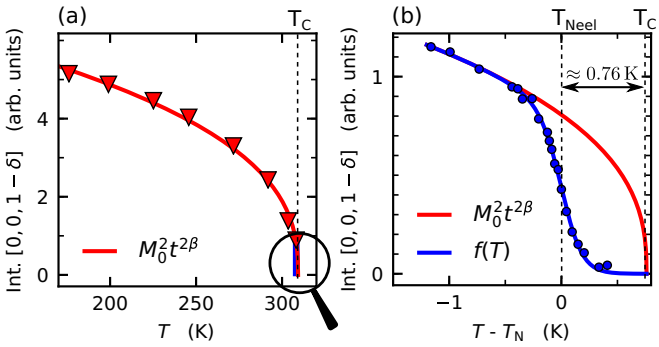

FIG. 1. T dependence of the $(0, 0, 1-\delta)$ magnetic satellite peak $I(T)$ of Cr [22]. (a) On a coarse T scale, the data points from Ref. [22] can be parametrized assuming a second-order phase transition with $I(T) \propto t^{2\beta}$ (red line). (b) The enlargement of $I(T)$ close to T_N reveals a weak first-order phase transition [21]. The solid blue line is an empirical fit to the data from Ref. [21], taking all shown data points into account. The fitting function, Eq. (1), is explained in Sec. IV.

would change from first to second order and a tricritical point is expected at a critical pressure $p_{[110]} = p^{\text{crit}}_{[110]}$ [11].

A first attempt to investigate Cr under uniaxial pressure was performed by Fawcett *et al.* [21]. However, the prediction of Barak *et al.* could be neither verified nor falsified because the Néel transition began to broaden irreversibly for pressures in the range $160 \text{ bar} \leqslant p_{[110]} \leqslant 300$ bar. Fawcett *et al.* conjectured that the broadening was caused by the formation of residual stresses due to the occurrence of plastic deformation [21]. To draw definite conclusions concerning the possibility of inducing a second-order phase transition by uniaxial pressure we have designed an improved pressure cell that allows the performance of experiments under controlled conditions for pressures exceeding $p_{[110]} = p^{\text{crit}}_{[110]}$.

The magnetic properties of Cr may be summarized as follows: Nesting of the Fermi surface leads to the formation of a sinusoidal incommensurate SDW with ordering vectors $\mathbf{Q}_\pm = (2\pi/a)(0, 0, 1 \pm \delta)$, where $a = 2.88$ Å is the lattice constant and $\delta = 0.048$ [22]. A spin-flop transition from the longitudinal to the transverse SDW phase takes place at $T_{\text{SF}} = 121$ K. At the Néel temperature $T_N = 311$ K, Cr enters the paramagnetic phase via a weak first-order phase transition. The incommensurate ordering leads to a complicated spectrum of magnetic excitations which emerges from the magnetic satellites and is still not understood [23] despite intense experimental and theoretical efforts [24].

In contrast to most ferro- and antiferromagnets, which enter the paramagnetic phase via a continuous second-order phase transition, Cr exhibits a weak first-order phase transition as mentioned above. Figure 1(a) depicts the temperature dependence of the intensity of the magnetic satellite peak near the Néel temperature T_N, the intensity of which is proportional to the square of the staggered magnetization M [22]. Assuming a second-order phase transition, the data points are fitted with the expression $M^2 = M_0^2 t^{2\beta}$, where the reduced temperature is given by $t = (T_c - T)/T_c$, yielding $\beta = 0.19 \pm 0.01$ and a putative transition temperature $T_c = T_N + (0.76 \pm 0.14)$ K, which exceeds the experimentally determined T_N. Zooming into the region near T_N reveals that the phase transition is indeed weakly first order as indicated by the blue circles in Fig. 1(b) [21].

We have used an improved design of the uniaxial pressure cell that was developed by Chacón *et al.* [25] based on work reported in Ref. [26]. It was successfully applied to characterize the dependence of the magnetic order of MnSi on uniaxial pressure [27]. Adams *et al.* used the same pressure cell in an experiment on Cr, where the pressure was applied along the [001] crystallographic direction [28].

The value of the critical pressure $p^{\text{crit.}}_{[110]}$ is not predicted by Barak's model due to unknown material constants. However, we have shown that the application of a uniaxial pressure of 600 bar along the [001] direction is already sufficient to completely suppress the SDW satellites along [001] [28]. As a rough guess we assume that 600 bar along [110] may also be sufficient to suppress the four magnetic reflections $[\pm\delta, \pm\delta, 1]$. Because the suppression of magnetic Bragg peaks is supposed to coincide with the extinction of the associated fluctuations, we conjecture that $p^{\text{crit.}}_{[110]} \approx 0.6$ kbar.

II. IMPLICATIONS OF STRESS INHOMOGENEITIES

Uniaxial pressure cells are a formidable tool to study effects of magnetoelastic coupling in antiferromagnetic materials [21,29]. As discussed above, the application of 0.6 kbar along the [001] direction may be sufficient to completely suppress the magnetic Bragg peaks $[0, 1, \pm\delta]$ [28]. This pressure corresponds to the application of only 60 N on a cross-sectional area of 1 mm^2.

A disadvantage of applying uniaxial pressure in comparison to an externally applied magnetic field is the presence of pressure inhomogeneities in the sample, which are difficult to control. A discussion of the dependence of the stress inhomogeneities as a function of the dimensions of the sample and the mechanical deficiencies of the pressure cells may be found in Ref. [30].

Typically, pressure inhomogeneities lead to a smearing of phase transitions. Using the experimentally determined value $dT_N/dp_{[110]} = -1.5 \pm 0.4$ K/kbar for Cr [21], the shift of the transition temperature $T_c - T_N = 0.76$ K corresponds to a uniaxial pressure $p_{[110]} = 510$ bar. Therefore, it must be verified that the standard deviation σ_p of the uniaxial pressure within the sample is $\sigma_p \ll 510$ bar.

Plastic deformation of a sample sets in when the von Mieses stress, $\sigma_{\text{mis}} := [\frac{1}{2}((\sigma_{xx} - \sigma_{yy})^2 + (\sigma_{yy} - \sigma_{zz})^2 + (\sigma_{zz} - \sigma_{xx})^2) + 3(\sigma_{xy}^2 + \sigma_{xz}^2 + \sigma_{yz}^2)]^{1/2}$, exceeds the yield strength, σ_{yield} [31]. For typical sample dimensions, all components except σ_{zz} may be neglected [30], yielding $\sigma_{\text{mis}} \approx |p_{[110]}|$. However, stress inhomogeneities lower the threshold for plastic deformation. On a $2\sigma_p$ tolerance level, plastic deformation starts when the mean pressure $\bar{p}_{[110]}$ exceeds the threshold $\sigma_{\text{yield}} - 2\sigma_p$.

III. EXPERIMENTAL SETUP

The Cr sample under investigation had the shape of a prism of height $h = 7.56$ mm and a square cross section with sides $a = 2$ mm. It was cut from a cylindrical single crystal purchased from Johnson-Matthey Co. The crystal was grown

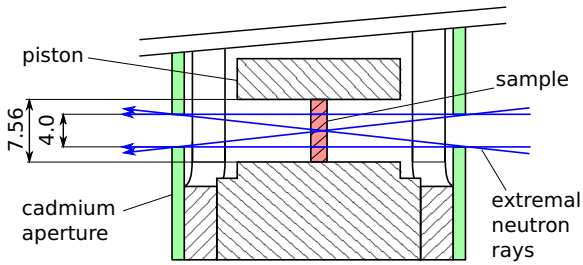

FIG. 2. Cross-sectional view of the lower part of the pressure cell. The sample is indicated by the vertical red rectangle. Cadmium sheets (green rectangles) have been wrapped around the sample cage and leave windows with a height of 4 mm. The window clips the St. Venant region [30].

using the same Czochralski growth process as used for the samples of Hiraka *et al.* [23,32]. The sample mosaic was $\eta = 40'$.

One component of the stress errors is caused by barreling. It can be shown that these errors concentrate near the contact surface and become exponentially weaker as a function of the z coordinate [30]. Our choice of h/l guarantees that average stress errors caused by barreling are below 10%, if boundary regions with a height of at least 1.6 mm are clipped using cadmium apertures. Exceeding this estimate we used apertures that reduce the neutron beam by approximately 1.8 mm on each side (Fig. 2).

Another important component of the stress errors is caused by bending of the sample, which is caused by nonparallel contact surfaces if standard, guided pistons are used. In order to minimize stress inhomogeneities caused by nonparallel contact surfaces we used a piston that compensates inclinations as proposed by Schade using grease as lubricant [30]. For our design of the piston that compensates for inclinations we postulate that the bending of the sample mostly depends on the centering of the sample in the apparatus, while the surface inclination is of lesser importance. We estimate that the centering error of the sample is bounded by $\Delta d < 0.2$ mm, and thus the stress error caused by eccentricity is below 2%. The above considerations suggest a total error in the stress of $\approx 12\%$. Nevertheless, our setup cannot guarantee that the stress errors are less than 12%, since other factors could contribute such as finite manufacturing and alignment tolerances and residual friction between the piston and the sample despite the use of low-friction lubricants [30].

Elastic neutron scattering experiments were conducted at MIRA (FRM II) [33,34] in the triple-axis mode with an energy transfer $\Delta E = 0$. Stress was applied using a He-activated uniaxial pressure cell [27]. A manometer records continuously the helium pressure in the gas bellow. The applied stress is then determined using the effective area of the metal bellow and the sample dimensions, yielding an accuracy for the pressure of better than 1% within the temperature range investigated (305.5 K $\leqslant T \leqslant$ 312 K). We performed 12 temperature sweeps during which we repeatedly measured the integral intensity of the magnetic Bragg peak $[0, 0, 1 - \delta]$ using a longitudinal scan in reciprocal space as shown in Fig. 3. Each sweep started at a temperature $T_1 > T_N$ followed by a decrease in T at a constant rate of 2.7 K/h to $T_2 < T_N$.

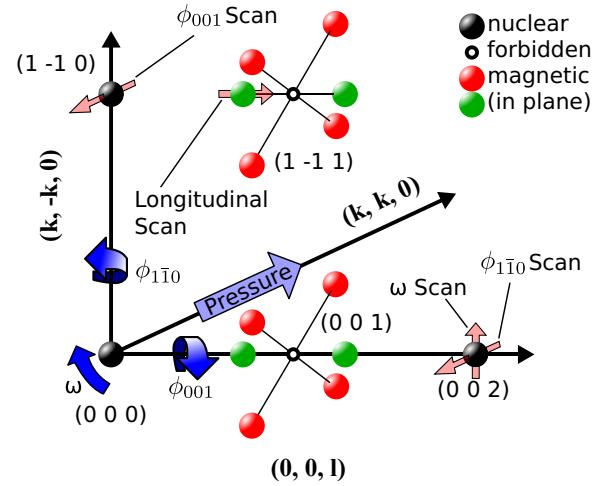

FIG. 3. Scattering plane in reciprocal space. The uniaxial pressure is applied along [110], i.e., normal to the scattering plane. The longitudinal scan is used to measure the magnetization as a function of the temperature, and the ω, $\phi_{1\bar{1}0}$, and ϕ_{001} scans are used for realigning the sample after each pressure change.

After each pressure change, we optimized the orientation of the sample to compensate for possible tilting of the crystal planes due to a rigid rotation or a plastic deformation by adjusting the angles ω, $\phi_{1\bar{1}0}$, and ϕ_{001} (see Fig. 3). For this purpose the intensity of the nuclear Bragg peaks $[1, -1, 0]$ and $[0, 0, 2]$ was optimized.

Figure 4 shows the optimized goniometer angles ω, $\phi_{1\bar{1}0}$, and ϕ_{001} for each pressure. It is shown that the angles ω and ϕ_{001} do not change significantly. In contrast, $\phi_{1\bar{1}0}$ decreases strongly by about 0.5° for $p_{[110]} \geqslant 550$ bar. We see below that the strong tilting of the (001) crystal planes about the $[1\bar{1}0]$ axis is linked to the observed plastic deformation of the crystal.

IV. EXPERIMENTAL RESULTS

Figure 5 summarizes the 12 temperature sweeps we performed. They are numbered in the sequence of occurrence.

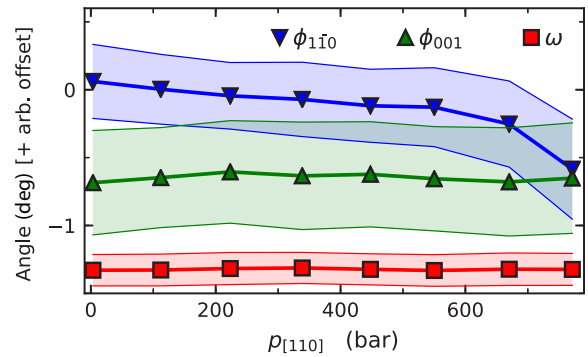

FIG. 4. Orientation of the scattering plane parameterized by the angles $\phi_{1\bar{1}0}$, ϕ_{001}, and ω as a function of the applied uniaxial pressure. Error bars are smaller than the symbol size. The shading indicates the full width at half-maximum of the Bragg peaks used for the alignment (Fig. 3).

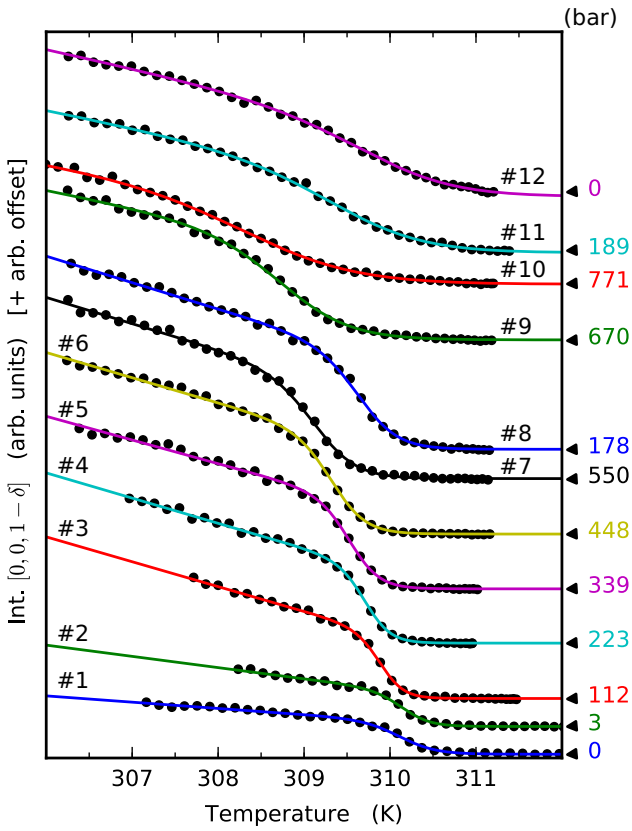

FIG. 5. Summary of all temperature sweeps performed. The numbering #1 to #12 reflects the sequence of the measurements. Data sets are shifted vertically by a constant for better visibility. The scaling of the intensity axis is the same for each curve. Error bars are smaller than the size of the symbols. Solid lines depict the fitted function $f(T)$ given by Eq. (1). The numbers on the right-hand axis indicate the applied pressure in bars.

From #1 to #7 the uniaxial pressure was monotonically increased from 0 to 550 bar. In run #1 the piston had no mechanical contact with the sample. The data show that the smearing of the phase transition does not change significantly. However, the step height increases by a factor of approximately 3, indicating a complete population of the SDW domain with $\mathbf{Q}_\pm$ parallel to [001]. There is also an indication of a lowering of T_N by ≈ 0.8 K with increasing pressure, quantitatively consistent with the known pressure dependence of T_N. Within the accuracy of our experiments we did not observe a change in the incommensurability δ.

Subsequently decreasing the pressure from 550 to 178 bar (run #8) essentially resulted in a shift in the data of run #7 to a higher temperature without involving a significant change in the profile. This result indicates (i) that the sample behaved reversibly and (ii) that the sample remained in a single-$\mathbf{Q}_\pm$ state. During the course of runs #9 and #10 the pressure was increased further before it was reduced again to 0 bar (#11, #12). The data clearly show a significant broadening of the transition that is irreversible. We conclude that the sample was plastically deformed.

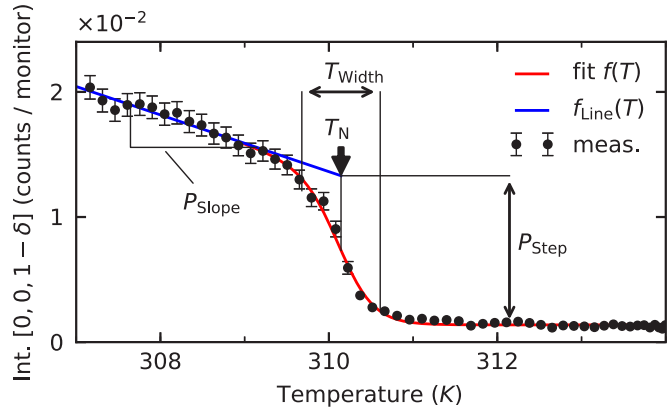

FIG. 6. Fit of data set #1 (0 bar) by $f(T)$ from Eq. (1). The width of the transition, T_{Width}, is approximately given by the [10% × P_{Step}, 90% × P_{Step}] levels. Error bars represent the confidence interval of 2σ. They are not shown if they are smaller than the size of the symbols.

For a quantitative estimate we parametrized the data by the function $f(T)$ given by

$$f(T) = f_{\mathrm{Line}}(T) \times f_{\mathrm{Sigmoid}}(T) + P_{bg}, \tag{1}$$

where

$$f_{\mathrm{Line}}(T) := P_{\mathrm{Slope}} \times (T - T_N) + P_{\mathrm{Step}}, \tag{2}$$

$$f_{\mathrm{Sigmoid}}(T) := \frac{1}{1 + \exp\left(\frac{T - T_N}{\Delta T}\right)}, \tag{3}$$

$$\Delta T := \frac{T_{\mathrm{Width}}}{2 \log 9}. \tag{4}$$

Here, P_{bg}, P_{Slope}, P_{Step}, T_N, and T_{Width} are the fit parameters designating the background, the linear slope of the integrated intensity of the magnetic peak, the increase in the intensity at the phase transition, the Néel temperature, and the width of the transition, respectively (see Fig. 6). The choice of $f_{\mathrm{Sigmoid}}(T)$ in the form of a Fermi function is purely empirical.

V. DISCUSSION

The pressure dependence of P_{Step} shown in Fig. 7 confirms the conclusions drawn from the raw data notably that a single $\mathbf{Q}_\pm$ state is populated at the high pressure of $p_{[110]} \approx 448$ bar. There is an indication of a downturn of P_{Step} at 771 bar, which does not recover when the pressure is released, suggestive of plastic deformation.

Figure 8 shows that T_N decreases linearly as long as $p_{[110]} \leqslant 550$ bar. Above 550 bar, T_N decreases more rapidly, indicating the development of stress inhomogeneities, i.e., $\sigma_p > 0$. A linear regression of the slope yields

$$\frac{dT_N}{dp} = (-1.77 \pm 0.10)\,\frac{\mathrm{K}}{\mathrm{kbar}}. \tag{5}$$

In addition to the statistical error of the fit, a systemic error of 0.012 K/kbar due to the pressure calibration is included.

The slope as determined in our experiment is in good agreement with the slope determined by Fawcett *et al.*, who obtained $dT_N/dp = -1.5 \pm 0.4$ K/kbar [21]. It compares

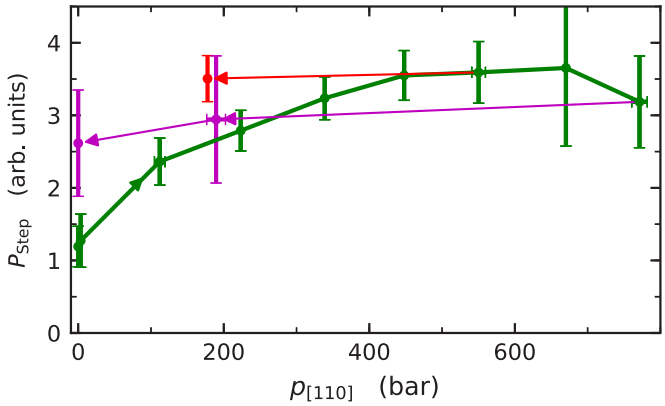

FIG. 7. Increase in the intensity of the magnetic satellite peak $(0, 0, 1-\delta)$ at T_N versus $p_{[110]}$. With increasing $p_{[110]}$, P_{Step} increases. After reaching 550 and 771 bar, $p_{[110]}$ was reduced to 178 bar (red arrow) and 0 bar (violett arrow), respectively. Irreversibilities are observed for $p_{[110]} \geqslant 550$ bar.

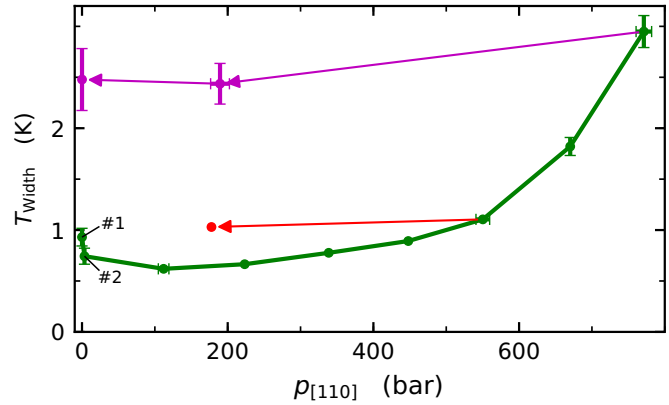

FIG. 9. Width of the Néel transition, T_{Width}, versus $p_{[110]}$. After reaching 550 and 771 bar, $p_{[110]}$ was reduced to 178 bar (red arrow) and 0 bar (violet arrow), respectively. Irreversibilities are observed for $p_{[110]} \geqslant 550$ bar. Error bars are omitted when they are smaller than the symbol size. Data points with the labels #1 and #2 correspond to sweeps #1 (0 bar) and #2 (3 bar).

well also with the slope as reported by McWhan and Rice [35] under application of hydrostatic pressure; they found $(dT_N/dp)_{\mathrm{iso}} = -5.1\ \frac{\mathrm{K}}{\mathrm{kbar}}$, which is $\simeq 2.9$ times larger than our value, i.e., very close to the theoretical value of 3. For more recent results on Cr under hydrostatic pressure see the work by Jaramillo *et al.* [36].

Finally, Fig. 9 shows the central result of our investigation, namely, the pressure dependence of the width of the transition. Initially, T_{Width} shrinks significantly, from 0.93 K at 0 bar (sweep #1) to 0.62 K at 3 bar, before increasing again and assuming, at $p_{[110]} \approx 448$ bar, the value of sweep #1. At higher pressures, $p_{[110]} \geqslant 550$ bar, T_{Width} increases rapidly. When releasing $p_{[110]}$ in this regime, T_{Width} maintains its high value, suggesting plastic deformation. The signature of a tricritical point, as predicted by Barak *et al.* [11], would be reflected in a marked and *reversible* increase in T_{Width} as typically observed for a continuous phase transition. This is not observed.

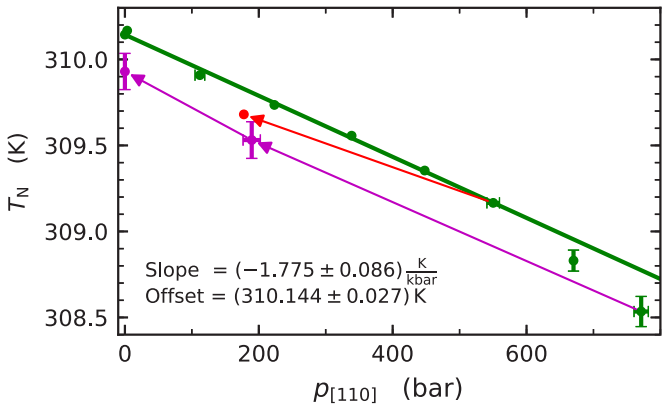

FIG. 8. Néel temperature T_N versus $p_{[110]}$. After reaching 550 and 771 bar, $p_{[110]}$ was reduced to 178 bar (red arrow) and 0 bar (violet arrow), respectively. Irreversibilities are observed for $p_{[110]} \geqslant 550$ bar. Error bars are omitted when they are smaller than the symbol size.

In the experiment reported by Fawcett *et al.* [21], the width of the transition was found to increase by a factor of approximately 2 between 160 and 300 bar, in contrast to our experiment, where a significant broadening occurs only above 550 bar. We attribute the behavior of our sample to the significantly more homogeneous stress distribution.

Finally, let us discuss the width of the magnetic phase transition in Cr at zero pressure. The data points labeled #1 and #2 in Fig. 9 correspond to sweeps #1 ($p_{[110]} = 0$ bar) and #2 ($p_{[110]} = 3$ bar). As soon as the piston comes into contact with the sample, T_{Width} is significantly reduced, by about 0.2 K, while a significant difference in T_{N} and T_{Step} between sweep #1 and sweep #2 is not observed. The decrease in T_{Width} may be a consequence of an improved alignment of $\mathbf{Q}_{\pm}$ perpendicular to $p_{[110]}$ due to the applied pressure. According to Eq. (5) a pressure difference $\triangle p \simeq 110$ bar is required to shift T_N by 0.2 K, which is much higher than the applied pressure of 3 bar in sweep #2. Therefore, the width of the transition at T_N at zero pressure, $T_{\mathrm{Width}} \approx 0.93$ K, is intrinsic (maybe caused by imperfections of the crystal) and is not caused by residual stress in the sample.

When the pressure is released from 550 bar (#7) to 178 bar (#8) T_N increases, however, T_{Width} remains essentially constant, clearly indicating that irreversibilities occur. A similar scenario is observed when $p_{[110]}$ is further increased to 771 bar (#10) and released to zero pressure (#12).

VI. SUMMARY AND OUTLOOK

Based on our experimental results, namely, that the transition at T_N remains first order, we rule out the existence of a tricritical point in Cr for uniaxial pressures $p_{[110]} \leqslant 550$ bar despite the observation that the sample is obviously in a single-$\mathbf{Q}_{\pm}$ state above 448 bar (Fig. 7). Reaching 550 bar is a significant improvement in comparison to previous work in which no broadening was observed up to only 160 bar [21]. As a precondition for this conjecture, we succeeded in reducing the stress inhomogeneities strongly in our setup.

Comparing our results with a similar study on MnO by Bloch *et al.* [37] we hesitate to rule out the appearance of a tricritical point in Cr under controlled uniaxial pressure exceeding $p_{[110]} > 550$ bar. Bloch *et al.* observed that a significant detwinning occurred in MnO at $p = 1.2$ kbar, while clear evidence of tricritical behavior was only observed at a pressure $p = 5.5$ kbar [37]. Therefore, our uniaxial pressure device should be improved further to reach uniform pressures higher than 550 bar.

In contrast to Cr, where magnetostrictive effects are extremely small, i.e., $\triangle d/d \simeq 1 \times 10^{-5}$ [38], a strong spontaneous contraction of the lattice occurs in the ordered phase of antiferromagnetic MnO, i.e., the angle between the [100] and the [010] axis becomes 1.12×10^{-2} rad at 4 K. [37] Therefore one may speculate that in the presence of the strongly enhanced magnetic fluctuations reported by Sternlieb *et al.* at the silent satellite positions in Cr close to T_N [39] and the extremely small magnetostrictive effects, the phase space for magnetic fluctuations in Cr is not reduced when uniaxial pressure forces Cr to become single $\mathbf{Q}_{\pm}$. Hence, a stress-induced tricritical point in Cr may not exist and the phase transition in Cr remains weakly first order.

ACKNOWLEDGMENTS

We gratefully acknowledge the technical support from R. Schwikowski, A. Mantwill, and the team of FRM II. We thank G. Brandl and E. Faulhaber for their support with the computer infrastructure at MIRA. We gratefully acknowledge financial support through DFG TRR 80 (From Electronic Correlations to Functionality).

[1] D. A. Sokolov, N. Kikugawa, T. Helm, H. Borrmann, U. Burkhardt, R. Cubitt, J. S. White, E. Ressouche, M. Bleuel, K. Kummer, A. P. Mackenzie, and U. K. Rössler, Nat. Phys. **15**, 671 (2019).
[2] S. Mühlbauer, B. Binz, F. Jonietz, C. Pfleiderer, A. Rosch, A. Neubauer, R. Georgii, and P. Böni, Science **323**, 915 (2009).
[3] S. A. Brazovskii, Zh. Eksp. Teor. Fiz. **68**, 175 (1975) [Sov. Phys.-JETP **41**, 85 (1975)].
[4] S. A. Brazovskii, I. E. Dzyaloshinskii, and B. G. Kukharenko, Zh. Eksp. Teor. Fiz. **70**, 2257 (1976) [Sov. Phys.-JETP **43**, 1178 (1976)].
[5] M. Janoschek, M. Garst, A. Bauer, P. Krautscheid, R. Georgii, P. Böni, and C. Pfleiderer, Phys. Rev. B **87**, 134407 (2013).
[6] P. Böni, J. H. Bilgram, and W. Känzig, Phys. Rev. A **28**, 2953 (1983).
[7] U. Dürig, J. H. Bilgram, and W. Känzig, Phys. Rev. A **30**, 946 (1984).
[8] D. Mukamel and S. Krinsky, Phys. Rev. B **13**, 5065 (1976).
[9] P. Bak, S. Krinsky, and D. Mukamel, Phys. Rev. Lett. **36**, 52 (1976).
[10] P. Bak and D. Mukamel, Phys. Rev. B **13**, 5086 (1976).
[11] Z. Barak and M. B. Walker, J. Phys. F: Met. Phys **12**, 483 (1982).
[12] P. Bak and M. H. Jensen, J. Phys. C **13**, L881 (1980).
[13] A. Arrott, S. A. Werner, and H. Kendrick, Phys. Rev. Lett. **14**, 1022 (1965).
[14] Y. Ishikawa, T. Komatsubara, and D. Bloch, Physica B+C **86–88**, 401 (1977).
[15] A. Bauer, M. Garst, and C. Pfleiderer, Phys. Rev. Lett. **110**, 177207 (2013).
[16] S. S. Samatham and V. Ganesan, Phys. Status Solidi RRL **7**, 184 (2013).
[17] C. Pappas, L. J. Bannenberg, E. Lelièvre-Berna, F. Qian, C. D. Dewhurst, R. M. Dalgliesh, D. L. Schlagel, T. A. Lograsso, and P. Falus, Phys. Rev. Lett. **119**, 047203 (2017).
[18] Y. Nii, A. Kikkawa, Y. Taguchi, Y. Tokura, and Y. Iwasa, Phys. Rev. Lett. **113**, 267203 (2014).
[19] Z. Barak, E. Fawcett, D. Feder, G. Lorincz, and M. B. Walker, J. Phys. F **11**, 915 (1981).
[20] E. Fawcett, R. B. Roberts, R. Day, and G. K. White, Europhys. Lett. **1**, 473 (1986).
[21] E. Fawcett, D. Feder, W. C. Muir, and C. Vettier, J. Phys. F: Met. Phys. **14**, 1261 (1984).
[22] E. Fawcett, Rev. Mod. Phys. **60**, 209 (1988).
[23] H. Hiraka, P. Böni, K. Yamada, S. Park, S.-H. Lee, and G. Shirane, Phys. Rev. B **70**, 144413 (2004).
[24] R. S. Fishman and S. H. Liu, Phys. Rev. B **54**, 7252 (1996).
[25] A. Chacón Roldán, Bachelor's thesis, Technical University of Munich (2009).
[26] S. Waffenschmidt, C. Pfleiderer, and H. v. Löhneysen, Phys. Rev. Lett. **83**, 3005 (1999).
[27] A. Chacón, A. Bauer, T. Adams, F. Rucker, G. Brandl, R. Georgii, M. Garst, and C. Pfleiderer, Phys. Rev. Lett. **115**, 267202 (2015).
[28] T. Adams, G. Brandl, A. Chacón, J. N. Wagner, M. Rahn, S. Mühlbauer, R. Georgii, C. Pfleiderer, and P. Böni, Appl. Phys. Lett. **105**, 123505 (2014).
[29] B. Hälg, W. Berlinger, and K. Müller, Nucl. Instrum. Methods A **253**, 61 (1986).
[30] A. Schade, Master's thesis, Technical University of Munich (2016) .
[31] R. Hill, *The Mathematical Theory of Plasticity* (Oxford University Press, New York, 1998), pp. 19–23.
[32] H. Hiraka, Y. Endoh, P. Böni, M. Fujita, K. Yamada, and G. Shirane, Phys. Rev. B **67**, 064423 (2003).
[33] R. Georgii, T. Weber, G. Brandl, M. Skoulatos, M. Janoschek, S. Mühlbauer, C. Pfleiderer, and P. Böni, Nucl. Instrum. Methods A **881**, 60 (2018).
[34] R. Georgii and K. Seemann, JLSRF **1**, A3 (2015).
[35] D. B. McWhan and T. M. Rice, Phys. Rev. Lett. **19**, 846 (1967).
[36] R. Jaramillo, Y. Feng, J. Wang, and T. F. Rosenbaum, Proc. Natl. Acad. Sci. USA **107**, 13631 (2010).
[37] D. Bloch, D. Hermann-Ronzaud, C. Vettier, W. B. Yelon, and R. Alben, Phys. Rev. Lett. **35**, 963 (1975).
[38] F. H. Combley, Acta Crystallogr. B **24**, 142 (1968).
[39] B. J. Sternlieb, J. P. Hill, T. Inami, G. Shirane, W.-T. Lee, S. A. Werner, and E. Fawcett, Phys. Rev. Lett. **75**, 541 (1995).